The Journal of Chemical Physics ARTICLE pubs.aip.org/aip/jcp

Polyatomic radiative association by quasiclassical trajectory calculations: Formation of HCN and HNC molecules in H + CN collisions

Cite as: J. Chem. Phys. 159, 144112 (2023); doi: 10.1063/5.0170577
Submitted: 3 August 2023 • Accepted: 21 August 2023 •
Published Online: 13 October 2023

Péter Szabó[1,2,3,a] and Magnus Gustafsson[3,b]

AFFILIATIONS

[1] Department of Chemistry, KU Leuven, Celestijnenlaan 200F, 3001 Leuven, Belgium
[2] Royal Belgian Institute for Space Aeronomy (BIRA-IASB), Avenue Circulaire 3, 1180 Brussels, Belgium
[3] Applied Physics, Division of Materials Science, Department of Engineering Science and Mathematics, Luleå University of Technology, 97187 Luleå, Sweden

Note: This paper is part of the 2023 JCP Emerging Investigators Special Collection.
[a] **Author to whom correspondence should be addressed:** peter88szabo@gmail.com
[b] **Electronic mail:** magnus.gustafsson@ltu.se

ABSTRACT

We have developed the polyatomic extension of the established [M. Gustafsson, J. Chem. Phys. **138**, 074308 (2013)] classical theory of radiative association in the absence of electronic transitions. The cross section and the emission spectrum of the process is calculated by a quasiclassical trajectory method combined with the classical Larmor formula which can provide the radiated power in collisions. We have also proposed a Monte Carlo scheme for efficient computation of ro-vibrationally quantum state resolved cross sections for radiative association. Besides the method development, the global potential energy and dipole surfaces for H + CN collisions have been calculated and fitted to test our polyatomic semiclassical method.

I. INTRODUCTION

In astronomical environments there are several physical and chemical processes which result in molecule production: (i) chemical exchange reactions in gas phase or on the surface of grains, (ii) collisions with electrons, and (iii) interaction of atoms and molecules with radiation. In complex-forming bimolecular collisions, the transient complex can be stabilized either by the collision of a third body or by emitting a photon (see Fig. 1). The latter process is called radiative association (RA) and it contributes to molecule formation in dust-poor regions of interstellar space.[1,2]

Owing to the very small probability of spontaneous photon emission, it is difficult to measure the cross section and rate constant of RA. Experimental studies have been carried out only for a few ionic systems.[3] That is why theoretical modeling of the dynamics of RA is often the only feasible way to obtain a reliable cross section or rate constant of the process.[2] Nevertheless, RA is also challenging to study theoretically since, in principle, it requires the quantum mechanical description of the time-dependent process. Due to the difficulty of quantum mechanical treatments, most of the previous dynamical calculations have focused merely on diatomic molecule formation.[4–36] There are only a few quantum dynamics studies where radiative association of triatomic molecules has been considered in full dimension including the following molecules:[37–44] HeH_2^+, H_3^-, HN_2^-, AlH_2^+, AlD_2^+, NaH_2^+, NaD_2^+, HCO^-, HCO. For other polyatomic cases, either reduced dimensional semiclassical dynamical calculations[45,46] or statistical rate theories[47–51] are applied to obtain their rate constant.

The extension of the theoretical models for polyatomic systems is desirable, since the bigger the reactants, the more probable the RA is.[47] Unfortunately, the quantum dynamical methods are not feasible for larger polyatomic molecules. However, the classical or semiclassical treatment of the dynamics can provide a practical but still efficient solution regardless of the size of reactants. Despite the lacking quantum effects, the trajectory-based method with a good quality potential energy surface can provide accurate rate

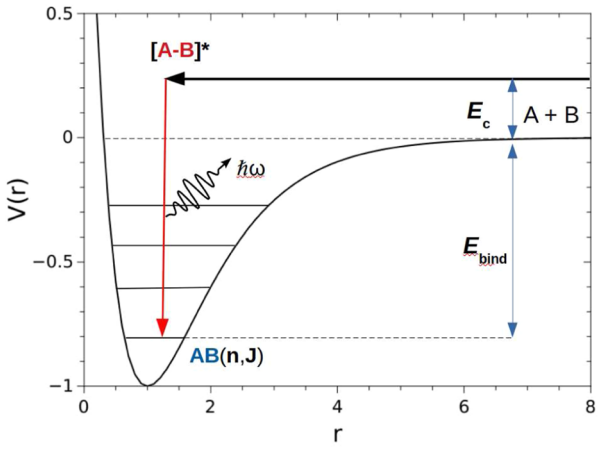

FIG. 1. Schematic representation of the radiative association process for the formation of a hypothetical AB(**n**, **J**) molecule in a given ro-vibrational quantum state characterized by a collection of vibrational quantum numbers, **n**, and angular momentum, **J**. E_c denotes the collision energy and E_{bind} is the binding energy of the molecule.

constants, spectral properties, and also reliable atomic-scale mechanism of molecular collisions.[52–62]

Two trajectory-based classical methods have been recently established for RA. One is for RA in absence of electronic transitions based on the classical Larmor theory of radiation,[63] and another for the calculation of RA through electronic transitions based on the semiclassical surface-hopping formalism.[64] Both methods are tested and used successfully to calculate the diatomic molecule formation through RA. However, these methods have not yet been extended for polyatomic systems to consider the dynamics in full dimension.

The purpose of this work is to develop and implement the polyatomic extension of the earlier established method for RA in absence of electronic transitions.[63] In order to test our method we calculate the cross sections of the following reaction:

$$\mathrm{H}\left(^2S\right) + \mathrm{CN}\left(^2\Sigma^+\right) \rightarrow \mathrm{HCN/HNC} + \hbar\omega \tag{1}$$

Besides the dynamical studies, we also develop a global *ab initio* potential energy surface (see Fig. 2) and a dipole surface for H + CN collisions.

HCN and HNC molecules are fundamental building blocks for the synthesis of more complex nitrogen bearing molecules.[65,66] They have been detected in various regions of the interstellar medium

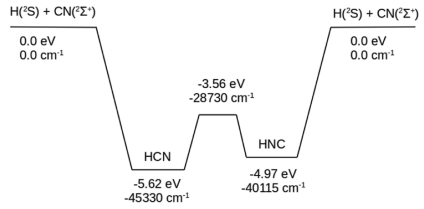

FIG. 2. Schematic representation of ground state H + CN potential energy surface.

including star-forming regions,[66–72] nebulae, planetary nebulae, circumstellar envelopes and disks, and comets. HCN and HNC are assumed to form primarily through gas-phase chemistry,[73–76] and they are considered important tracers of molecular gas and high-density regions in the interstellar medium. Furthermore, their spectroscopic line intensities can be utilized as chemical thermometer for the interstellar medium.[77] Owing to the relevance of these molecule, it is important to unveil their possible formation pathways like the radiative association that might have a contribution to the production of HCN and HNC in the dust-poor interstellar space.

II. QUASICLASSICAL THEORY OF RADIATIVE ASSOCIATION

According to the recently developed method,[63] the cross section of the radiative association can be computed by using a combination of the classical trajectory method and the Larmor formula in which the spontaneous emission is a result of a time-dependent dipole. The method applies only in absence of electronic transitions, and it was tested so far only for diatomic molecule formation. As is presented earlier, this classical method can reproduce the resonance-free quantum mechanical cross sections with good accuracy. Here, we generalize this classical theory of radiative association[63] for an arbitrary polyatomic system by deriving the formula for quantum state resolved semiclassical cross section. Then we also give a Monte Carlo schemes for the efficient evaluation of the cross section. Note that in this work the term *semiclassical* refers to the semiclassical quantization of the rovibrational states of the reactants. This should not be confused with the semiclassical treatment of radiative association of diatomic molecules involving different electronic states.[78,79]

A. Derivation of cross section formula

Since radiative association is a collision process, its cross section can be obtained by the classical collision theory

$$\sigma(E_c) = 2\pi f_{\mathrm{stat}} \int_0^\infty b P_{\mathrm{r}}(E_c, b)\, \mathrm{d}b, \tag{2}$$

where P_{r} is the opacity function (the probability of the radiation as a function of impact parameter, b, and collision energy, E_c). The statistical weight factor, f_{stat} can be calculated from the spin- and orbital angular momentum multiplicity of the electronic quantum states of the reactants and product involved in the collision.

In the frequency interval $[\omega, \omega + \mathrm{d}\omega]$ the probability of emission is $I(\omega)\,\mathrm{d}\omega/\hbar\omega$. Hence, the total probability of radiation is

$$P_{\mathrm{r}} = \int_0^\infty \frac{I(\omega)}{\hbar\omega}\, \mathrm{d}\omega, \tag{3}$$

where $I(\omega)$ is the radiated energy per unit frequency. In the classical theory of dipole radiation, the time-dependent radiative power (the total energy radiated from the system per unit time) is given by the Larmor formula[80]

$$I(t) = -\frac{\mathrm{d}E}{\mathrm{d}t} = \frac{2}{3c^3 4\pi\epsilon_0} \ddot{\mathbf{D}}^2, \tag{4}$$

where E is the radiated energy, c is the speed of light, ϵ_0 is the permittivity of vacuum, and $\mathbf{D}$ is time-dependent dipole moment of

the system. By Fourier transforming Eq. (4) and using the Parseval theorem

$$\int_{-\infty}^{\infty} f_t^2 \, \mathrm{d}t = \int_{-\infty}^{\infty} |f_\omega|^2 \frac{\mathrm{d}\omega}{2\pi} = 2\int_{0}^{\infty} |f_\omega|^2 \frac{\mathrm{d}\omega}{2\pi}, \tag{5}$$

we obtain the frequency dependent radiated power as[80]

$$I(\omega) = \frac{2}{3c^3\pi 4\pi\epsilon_0} \left| \int_{-\infty}^{\infty} e^{i\omega t} \ddot{\mathbf{D}}(b,t,E_c)\mathrm{d}t \right|^2. \tag{6}$$

Inserting $I(\omega)$ into Eq. (3), the total radiative probability can be computed as

$$P_\mathrm{r} = \frac{2}{3c^3\pi\hbar 4\pi\epsilon_0} \int_{\omega_c}^{\omega_\mathrm{max}} \frac{1}{\omega} \left| \int_{-\infty}^{\infty} e^{i\omega t} \ddot{\mathbf{D}}(b,t,E_c)\mathrm{d}t \right|^2 \mathrm{d}\omega, \tag{7}$$

where the new boundaries of the frequency integral are introduced to take into account only the transitions which result in stable molecule formation. By having $\omega_c = E_c/\hbar$ as a lower limit, rather than 0, transitions to the continuum are excluded. Furthermore, $\omega_\mathrm{max} = E_\mathrm{max}/\hbar$, where E_max is the maximally possible energy loss of the system in the collision, corresponding to the minimum ro-vibrational energy and total angular momentum of the formed molecule. See Appendix A for further details of how to determine the value of E_max. For neutral systems, we may introduce further simplification by applying the differentiating property of Fourier transformation

$$|\mathcal{F}(\ddot{\mathbf{D}})|^2 = \omega^4 |\mathcal{F}(\mathbf{D})|^2, \tag{8}$$

with this identity

$$P_\mathrm{r} = \frac{2}{3c^3\pi\hbar 4\pi\epsilon_0} \int_{\omega_c}^{\omega_\mathrm{max}} \omega^3 \left| \int_{-\infty}^{\infty} e^{i\omega t} \mathbf{D}(b,t,E_c)\mathrm{d}t \right|^2 \mathrm{d}\omega. \tag{9}$$

It should be stressed that Eq. (9) is valid solely for neutral species. For ionic system P_r has to be calculated from Eq. (7) (see e.g., Öström *et al.*[20]). In such cases, the identity Eq. (8) does not hold because the dipole moment of ionic systems is not an L^2 (i.e., square integrable) function.

Equations (7) and (9) are suitable to describe merely the collision of two structureless fragments. In polyatomic reactions, the probability of the process also depends on the ro-vibrational states of the interacting partners. In the semiclassical picture these are characterized by a collection of initial (semiclassical) ro-vibrational quantum numbers $(\mathbf{n}_{AB})$ and the phases of rotations $(\boldsymbol{\eta})$ and vibrations $(\boldsymbol{\chi})$ of the reactants. Furthermore, the relative orientation of the colliding fragments, which is characterized by the Euler angles $(\boldsymbol{\psi})$, are also needed to be considered. Hence, in the general case (either ionic or neutral system), the polyatomic radiative probability density takes the form

$$P_\mathrm{r}^\mathrm{gen}(E_c, b, \mathbf{n}_{AB}, \boldsymbol{\eta}, \boldsymbol{\chi}, \boldsymbol{\psi}) = \frac{2}{3c^3\pi\hbar 4\pi\epsilon_0} \int_{\omega_c}^{\omega_\mathrm{max}} \frac{1}{\omega} \times \left| \int_{-\infty}^{\infty} e^{i\omega t} \ddot{\mathbf{D}}(b,t,E_c,\mathbf{n}_{AB},\boldsymbol{\eta},\boldsymbol{\chi},\boldsymbol{\psi})\mathrm{d}t \right|^2 \mathrm{d}\omega. \tag{10}$$

For neutral systems by using Eq. (8), Eq. (10) is simplified

$$P_\mathrm{r}^\mathrm{neut}(E_c, b, \mathbf{n}_{AB}, \boldsymbol{\eta}, \boldsymbol{\chi}, \boldsymbol{\psi}) = \frac{2}{3c^3\pi\hbar 4\pi\epsilon_0} \int_{\omega_c}^{\omega_\mathrm{max}} \omega^3 \times \left| \int_{-\infty}^{\infty} e^{i\omega t} \mathbf{D}(b,t,E_c,\mathbf{n}_{AB},\boldsymbol{\eta},\boldsymbol{\chi},\boldsymbol{\psi})\mathrm{d}t \right|^2 \mathrm{d}\omega. \tag{11}$$

Inserting Eqs. (10) and (11) into Eq. (2) and integrating over the phase variables $(\boldsymbol{\eta}, \boldsymbol{\chi}, \boldsymbol{\psi})$, we obtain the initial quantum state resolved semiclassical radiative association cross section for general and neutral polyatomic systems as

$$\sigma_\mathrm{gen}(E_c, \mathbf{n}_{AB}) = \frac{4f_\mathrm{stat}}{3c^3\hbar 4\pi\epsilon_0} \int_0^\infty b\,\mathrm{d}b \int_0^{2\pi} \cdots \int_0^{2\pi} \mathrm{d}\boldsymbol{\eta}\,\mathrm{d}\boldsymbol{\chi}\,\mathrm{d}\boldsymbol{\psi} \times \int_{\omega_c}^{\omega_\mathrm{max}} \frac{1}{\omega} \left| \int_{-\infty}^{\infty} e^{i\omega t} \ddot{\mathbf{D}}(b,t,E_c,\mathbf{n}_{AB},\boldsymbol{\eta},\boldsymbol{\chi},\boldsymbol{\psi})\mathrm{d}t \right|^2 \mathrm{d}\omega, \tag{12}$$

$$\sigma_\mathrm{neut}(E_c, \mathbf{n}_{AB}) = \frac{4f_\mathrm{stat}}{3c^3\hbar 4\pi\epsilon_0} \int_0^\infty b\,\mathrm{d}b \int_0^{2\pi} \cdots \int_0^{2\pi} \mathrm{d}\boldsymbol{\eta}\,\mathrm{d}\boldsymbol{\chi}\,\mathrm{d}\boldsymbol{\psi} \times \int_{\omega_c}^{\omega_\mathrm{max}} \omega^3 \left| \int_{-\infty}^{\infty} e^{i\omega t} \mathbf{D}(b,t,E_c,\mathbf{n}_{AB},\boldsymbol{\eta},\boldsymbol{\chi},\boldsymbol{\psi})\mathrm{d}t \right|^2 \mathrm{d}\omega. \tag{13}$$

One needs only to follow the time-dependent dipole moment of the system along its classical trajectory to calculate the ro-vibrationally state-resolved probability of spontaneous emission [Eqs. (10) and (11)] or the cross section [Eqs. (12) and (13)] of molecule formation in collisions.

B. Monte Carlo estimation of the cross section

Since the radiative probability, as well as the cross section, are many dimensional integrals Monte Carlo (MC) integration is needed for the efficient evaluation of Eqs. (10)–(13). To use the MC method one needs to sample randomly the initial conditions of reactants, including the ro-vibrational phases $(\boldsymbol{\eta}, \boldsymbol{\chi}) \in [0, 2\pi]$, the Euler angles $(\boldsymbol{\psi})$ and the impact parameter (b), to take into account all possible phase space points of colliding fragments that may have a contribution to the reaction.

When the phase variables are sampled uniformly and the impact parameter is sampled as $b_i = b_\mathrm{max}\sqrt{\xi_i}$, where $\xi_i \in [0, 1]$ is a uniform random number, then we obtain the following Monte Carlo formula

$$\sigma(E_c, \mathbf{n}_{AB}) \approx \frac{\pi b_\mathrm{max}^2}{N_\mathrm{tot}} \sum_i^{N_\mathrm{tot}} P_\mathrm{r}^{(i)}\left(E_c, \mathbf{n}_{AB}, b_i, \boldsymbol{\eta}_i, \boldsymbol{\chi}_i, \boldsymbol{\psi}_i\right) \tag{14}$$

for the initial quantum state resolved cross section for the collision of two arbitrary molecules, where $P_\mathrm{r}^{(i)}$ has to be calculated from Eq. (10) or Eq. (11) for the ith trajectory. In this MC scheme, each trajectory has a contribution to the total radiative probability.

III. COMPUTATIONAL DETAILS OF THE DYNAMICAL CALCULATIONS

A. Details of the quasiclassical trajectory calculations

The molecular collisions were studied using the quasiclassical trajectory (QCT) method. The calculations were performed using

an in-house built code, where the classical equations of motion are solved in Cartesian coordinates for each atom participating in the collision. To simulate the quantized nature of the vibration and rotation of the reactant molecules, the internal motion of molecules is described by ensembles of classical states that correspond to preselected quantum mechanical states. The magnitude of the rotational angular momentum of the CN molecule, L, was calculated from the conventional semiclassical quantization formula $L = \hbar\sqrt{(j(j+1)}$, where j is the rotational quantum number of the diatomic molecule. The ro-vibrational initial state of the CN molecule is sampled by employing a rotating Morse oscillator based on Porter–Raff–Miller method.[81] The impact parameter b was sampled with a weight proportional to b itself, and the maximum impact parameter was chosen dynamically as a function of the collision energy to take into account all reactive events. The Hamilton's equations of motion are integrated in Cartesian coordinates using the tenth-order Adams–Moulton predictor-corrector algorithm initiated by Velocity–Verlet integrator. The integration time step was 0.5 atomic time units in the calculations, guaranteeing energy conservation better than 0.5 cm^{-1} at the given collision energy. In this work, we have calculated 2×10^5 trajectories at each collision energy.

B. Details of the computation of radiative association cross section

In this section, we discuss the numerical issues and their solutions regarding the computation of the cross section. Along the trajectories, we recorded the time-dependent dipole of the system, which provides the starting point for the computation of the cross section. First, we discuss how to obtain efficiently the radiative probability for each trajectory and then how to use these individual probabilities to obtain the cross section.

1. Which dipole is supposed to be used and how?

In general, the non-interacting reactants possess a permanent dipole moment, such as that of CN in our case. This is illustrated in Fig. 4(a) by non-zero value of D_z when the H atom is far away, corresponding to the dipole of the free CN molecule. This means that rotating and vibrating molecules also radiate classically even before approaching the interaction zone in the collision. This effect should be removed from the recorded $\widetilde{\mathbf{D}}(t)$ because it does not result in molecule formation. Based on this consideration, the following modified dipole is used in Eq. (10)

$$\mathbf{D}(\mathbf{q},t) = \begin{cases} \widetilde{\mathbf{D}}_{\mathrm{eq}} & \text{if} \quad \mathbf{q} \notin [\text{int. zone}] \\ \widetilde{\mathbf{D}}(\mathbf{q},t) & \text{if} \quad \mathbf{q} \in [\text{int. zone}], \end{cases} \tag{15}$$

where $\widetilde{\mathbf{D}}_{\mathrm{eq}}$ is the constant value of the dipole of the non-interacting fragments at their equilibrium structure. $\widetilde{\mathbf{D}}_{\mathrm{eq}}$ is held at constant magnitude and direction so that it is time independent. In other words, outside the interaction zone $\mathbf{D}(\mathbf{q},t)$ has direction and magnitude that are independent of the CN orientation and bond length, respectively. Hence, outside the interaction zone, the second derivative of the dipole in Eq. (10) results in a zero contribution to the radiative power. In this work, the interaction zone is defined based on the Jacobi distance, where $R < 5.0$ Å. This is a reasonable choice since the dipole can be considered as constant above this value. Between $R_{\mathrm{min}} = 4.5$ Å and $R_{\mathrm{max}} = 5.5$ Å we used the switching function[82]

$$f_{\mathrm{sw}}(t) = \frac{1}{2} - \frac{1}{2}\tanh\left(\tan\left(\pi t\right)\right), \tag{16}$$

with the reduced variable

$$t = \frac{R - R_{\mathrm{min}}}{R_{\mathrm{max}} - R_{\mathrm{min}}} + \frac{1}{2}, \tag{17}$$

in order to obtain a smooth transition when we damp the dipole to the constant $\widetilde{\mathbf{D}}_{\mathrm{eq}}$. Furthermore, in Appendix B we give an alternative procedure to eliminate the radiation of the non-interacting reactants. In the present work, we tested both methods, and they resulted in the same cross section.

Besides the vibrational contribution of the radiation, it is also important to treat properly the rotation of the molecular complex. In our work, the dipole vector was written in Cartesian coordinates. Owing to this, the effect of rotation in the radiation process is automatically included. However, it should be stressed that the rotational contribution is not considered when the components of $\mathbf{D}(t)$ are expressed by internal coordinates. In such cases, one needs to use also the Euler-angles to take into account the change of dipole stemming from the time-dependent orientation of the collision-complex.

There is a further technical issue when the Cartesian component of the dipole is given in the frame of principal axis of inertia (PAI) – like the HCN/HNC system in the present work – and the dynamics is calculated in laboratory fixed Cartesian coordinates (LAB). In such cases, the dipole vector is supposed to be transformed from PAI to LAB coordinates in every time step of the trajectory by using the orthogonal transformation (rotation) matrix formed by the eigenvectors of the inertia tensor. However, the sign of the eigenvectors is not defined by the diagonalization which means there are eight different transformation matrices by considering the possible sign combinations. Such ambiguity may introduce discontinuity into the dipole in the LAB frame that is supposed to be used in Eqs. (10) and (11). A similar problem appears in reactive dynamics calculations, owing to the sign-ambiguity of the rotation matrix when the Eckart transformation is utilized to project out the rotational modes.[83] In order to avoid this numerical problem, we transformed the PAI dipole vector into LAB dipole vector by using all of the eight rotation matrices, and at the end, we chose that matrix where the obtained LAB dipole shows the largest overlap with the LAB dipole of the previous time-step. Since the inertia tensor has to be diagonalized in each time-step of dynamics we employed the special algorithm of Kopp[84] designed for 3×3 matrices.

2. Evaluation of the radiative probabilities

For the calculation of the cross section of neutral systems like the HCN molecule it would be rational to use Eq. (13) with Eq. (11). However, owing to the ω^3 factor in the frequency integral of Eq. (11), numerical issues may arise when the Fourier transform of the dipole is noisy. In our numerical experiments, the ω^3 factor amplified the numerical noise of the signal at large frequencies, which resulted in a no-convergent frequency integral for some trajectories. That is why Eq. (12) is recommended even for the characterization of

a neutral system instead of Eq. (13) because it always provides a convergent frequency integral thanks to the $1/\omega$ factor. However, using Eq. (12) demands the calculation of the second time derivative of dipole which may introduce additional noise into the spectrum. To reduce the numerical noise of the signal before Fourier transformation, we applied the Savitzky–Golay filter[85] on $\mathbf{D}(t)$ that automatically can provide the desired second derivative, $\ddot{\mathbf{D}}(t)$. In the Savitzky–Golay filter we applied a second order smoothed polynomial computed from the 5–5 data points in backward and forward direction.

There is another numerical obstacle, regarding the very long trajectories at low collision energies, which makes the evaluation of P_r in Eqs. (10) and (11) impossible. Based on the Nyquist condition, the maximum frequency that can be represented by Fourier transformation is $\omega_{top} \propto n_{FFT}/t_{traj}$, where n_{FFT} is the number of sampling points and t_{traj} is the integration time of the trajectory. This means that for very long trajectories, especially at low collision energies, the cut-off (ω_{top}) might be too small to represent properly the low-frequency part of the spectrum which has a significant contribution to the radiative probability. Based on the spectra of individual collision (see Fig. 8), in general at least $\omega_{top} = 10\,000\ \mathrm{cm}^{-1}$ is required in this reaction for the frequency integral in Eqs. (10) and (11). In principle, we could increase n_{FFT} to expand the cut-off frequency up to $\omega_{top} = 10\,000\ \mathrm{cm}^{-1}$. However, then it would not be feasible anymore to evaluate the Fourier transformation for all the trajectories within a reasonable computation time. Although we are not able to calculate P_r for such trajectories, we cannot discard them, since these collisions would have a considerable contribution to the cross section.

The radiative probability of these long trajectories is estimated as the maximum radiative power observed among all trajectories, where P_r can be computed from the Fourier transform of the time-dependent dipole. This estimation provides a conservative lower limit for the radiative probability of the extremely long trajectories and consequently establishes a lower bound for the computed classical radiative association cross sections.

Besides the integration of the equations of motion, the Fourier transformation is another computationally intensive numerical procedure in the calculation of radiative association. It is not useful to apply the same number of FFT sampling points for each trajectory, since the duration of the collisions can be quite diverse, and we do not need the spectrum at too high frequencies. To make more efficient the evaluation of P_r we dynamically adjusted n_{FFT} for each trajectory based on their integration time to make possible the representation of the emission spectrum at least up to $\omega_{top} = 10\,000\ \mathrm{cm}^{-1}$. The P_r of too long trajectories was not evaluated, instead estimated with the above-mentioned procedure, where we could not achieve at least $\omega_{top} = 10\,000\ \mathrm{cm}^{-1}$ with maximum $n_{FFT} = 2^{15}$.

IV. GLOBAL POTENTIAL ENERGY AND DIPOLE SURFACE OF H + CN SYSTEM

A. Details of the quantum chemical calculations

The Molpro package[86] was used for the quantum chemical calculations. The potential energy and the dipole moment surface are calculated with the explicit correlated internally contracted multireference configuration interaction method (icMRCI-F12) using the aug-cc-pVTZ-F12 basis set as implemented in Molpro. All calculations were carried out in the C_s point group. The reference wavefunction is obtained by using the state-averaged complete active space self-consistent field (CASSCF) method with a full valance active space, and with six states ($3A'$ and $3A''$) in the state average. The dipole moment of the system is calculated as an expectation value of the dipole operator.

In order to sample the configuration space of the system, we employed Jacobi coordinates of the HCN molecule denoted by (r_{CN}, R, θ). We used 19 points for $r_{CN} \in [0.8, 3.0]$ Å, 46 points for $R \in [0.5, 12.0]$ Å, and 25 points for $\theta \in [0°, 180°]$ to represent the configuration space.

B. Global potential energy surface

The calculated *ab initio* energies are interpolated by a 3D B-spline using the BSpline package.[87] The obtained PES is attractive, there is no barrier in the entrance channel (see Fig. 3). Over the range of the 3D spline fitting we employed the following extrapolation formulas

$$V_{sr}(r_{CN}, \theta, R) = ae^{-bR}, \tag{18}$$

which describes the short range part of the PES, and

$$V_{lr}(r_{CN}, \theta, R) = D_0 - C_6/R^6 \tag{19}$$

for the long-range extrapolation similarly as done by Ayouz *et al.*[88] The coefficients, a, b, D_0, C_6, are evaluated at each (r_{CN}, θ) value. The short range extrapolation parameters, a and b, are determined from two points: $V(r_{CN}, \theta, R = 0.50\ \text{Å})$ and $V(r_{CN}, \theta, R = 0.52\ \text{Å})$ at a given R, while the long-range parameters, D_0 and C_6 are obtained from $V(r_{CN}, \theta, R = 11.00\ \text{Å})$ and $V(r_{CN}, \theta, R = 11.80\ \text{Å})$ of the 3D spline potential values.

In order to test the quality of the PES, we used the DVR3D code[89] to compute the ro-vibrational quantum states. The results of these calculations are compared to the ro-vibrational energies of other works where the PES is developed for bound state spectroscopical calculations[90–95] (see Fig. S1 in the supplementary material). In general, the ro-vibrational energies of our PES slightly underestimate (by 10–15 cm^{-1}) the corresponding quantum states on most recent accurate PESs.[92–95] Such deviation is acceptable for global PESs which are used for collision dynamics and not solely

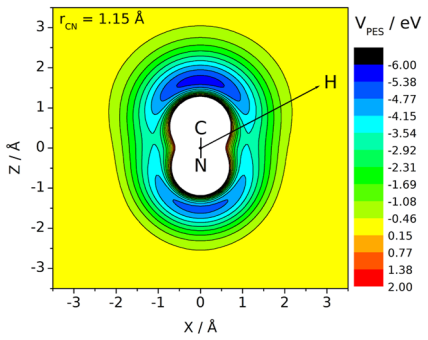

FIG. 3. Section of the PES of HCN at a fix r_{CN} distance.

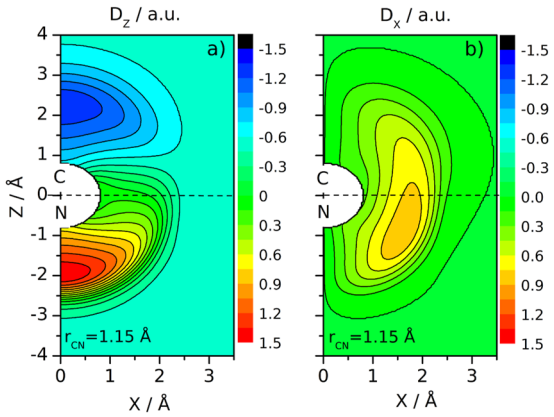

FIG. 4. Section of dipole surface of the HCN system. Panel (a) shows the *z*-component and panel (b) displays the *x*-component of the dipole.

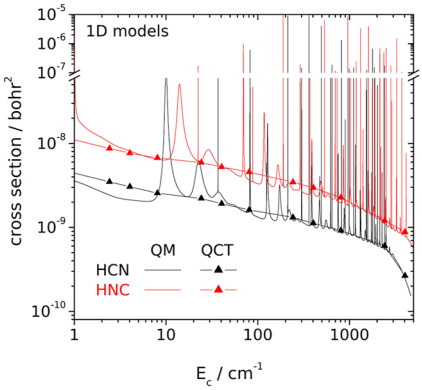

FIG. 5. Reduced dimensional (1D) cross section of the HCN and HNC formation in H + CN collisions obtained by quantum mechanical (QM) perturbation theory and the QCT method.

for bound state computations in order to describe the ro-vibrational spectroscopy with high accuracy.

C. Global dipole surface

Besides the PES, we also calculated and fitted the global electric dipole surface of the HCN system which is displayed in Fig. 4. The dipole vector is defined in the frame of principal axis of inertia (PAI) as in Molpro. The z component of the dipole is parallel with the CN bond and the x component is perpendicular to the CN bond. For the fitting procedure, we used the following function forms for the two PAI components of the dipole ($D_y = 0$, since all three atoms lie in the x, z plane)

$$D_x = \sum_{i=0}^{3}\sum_{j=0}^{6}\sum_{k=1}^{6} C_{ijk} r_{\mathrm{CN}}^{i} e^{-A_j(R-B_j)^2} P_k^1(\cos\theta), \tag{20}$$

$$D_z = \sum_{i=0}^{3}\sum_{j=0}^{6}\sum_{k=0}^{6} C_{ijk} r_{\mathrm{CN}}^{i} e^{-A_j(R-B_j)^2} P_k^0(\cos\theta), \tag{21}$$

where $P_k^m(\cos\theta)$ factors are the associated Legendre polynomials and A_j, B_j, C_{ijk} are parameters which are determined by nonlinear fitting. At long ranges ($R > 5.5$ Å) the dipole surface is extrapolated with the dipole of the free CN diatom. The comparison of the fitted dipole surface of the present work and that of Mourik *et al.*[90] can be found in Fig. S2 in the supplementary material. Around the equilibrium structures the two surfaces show a good agreement. However, the dipole surface of Mourik *et al.*[90] is represented only in a limited region of the configuration space that is useful for the calculation of spectral line intensities of a bound system, but not for the description of a collision process.

V. RESULTS AND DISCUSSION

A. Reduced dimensional QCT and quantum dynamics calculations

Besides the full dimensional QCT computations, we also performed reduced dimensional calculations in 1D by using our semiclassical QCT method and quantum mechanical (QM) perturbation theory. (See Appendix C for the computational details of QM.) For these calculations, we utilized the 1D sections of potential energy and dipole surfaces along the collinear H–CN and H–NC axes. Reduced-dimensional models serve as valuable tools for assessing the performance of classical or semiclassical methods in cases where full-dimensional quantum dynamical calculations are unavailable.[96,97] Furthermore, such comparison can shed light on the importance of missing degrees of freedom in the reduced dimensional treatment which have been applied previously to obtain the rate constant of polyatomic systems.[45,46]

Figure 5 shows the cross sections for the formation of HCN and HNC obtained by 1D reduced dimensional QCT and QM calculations. In complex-forming collisions when the tunneling is negligible, then the QCT method can remarkably well reproduce the baseline of the quantum dynamical cross section. Similar good agreement is observed for diatomic molecule formation when the capture is not hampered by a potential barrier in the entrance channel.

Based on this, we reckon here that the full dimensional QCT calculations can provide reliable cross sections for a wide range of collision energies apart from the resonances.

B. Full dimensional QCT calculations

The full-dimensional description of the RA process is highly desired, since there are several ro-vibrational degrees of freedom of polyatomic molecules that may contribute to the radiation process. QCT provides an efficient way to calculate the detailed dynamics of molecule formation through RA in arbitrary dimension when the global PES and dipoles surface is available.

The RA process is efficient when the system falls into the deep potential well, and the reactants spend several ro-vibrational periods together as a collision complex. That is why we calculated the radiative power only for complex-forming trajectories where the change of the dipole is considerable during the collision. The complex is defined by a geometric and energetic constraint: the center of mass of CN diatom and the hydrogen atom has to be closer than 4.5 Å,

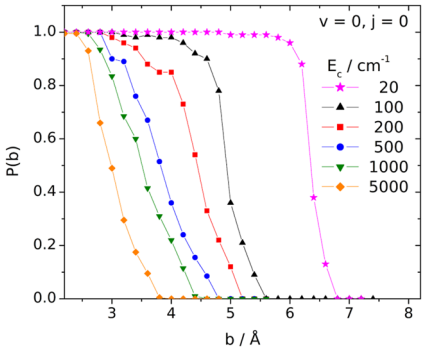

FIG. 6. Probability of complex formation (capture) as a function of impact parameter in H + CN collisions in full dimension.

and the potential energy has to reach at least half of the HCN potential well, −2.6 eV, at some point during the trajectory (see Fig. 3). Based on this definition, the non-complex-forming trajectories have negligible contribution to the radiated probability.

The opacity functions of complex formation are displayed in Fig. 6. The probability of capture is almost unity even at large impact parameters when the collision energy is low. This is a clear sign of the long-range attraction, which makes the capture more efficient under cold interstellar circumstances. The corresponding cross sections for complex formation (see in Fig. S3 in the supplementary material) show a divergent cross section as the collision energy diminishes.

The full dimensional RA cross section for the collision of $CN(v = 0, j = 0)$ and the hydrogen atom is shown in Fig. 7. It grows with decreasing energy, similar to the capture cross section, since at low collision energies the reactants spend more time together. Therefore, the probability of photon emission in the RA process is higher at cold temperatures. Figure 7 also clearly shows that the extremely long trajectories cannot be discarded. Trajectories with long lifetime have a considerable contribution to the reactivity. The cross section is larger with almost one order of magnitude at low and intermediate collision energies than those of obtained by omitting the trajectories with extremely long lifetime.

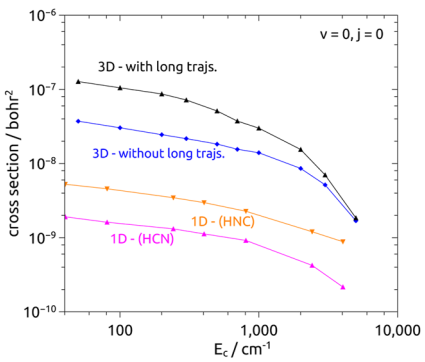

FIG. 7. Comparison of the reduced dimensional and 3D cross sections for the formation of HCN/HNC through radiative association.

In Fig. 7, we also present a comparison between the outcomes of the reduced-dimensional (1D) and full-dimensional QCT calculations. It is evident that the full-dimensional calculations yield a significantly larger cross section compared to the reduced-dimensional model. The difference spans almost two orders of magnitude across a wide range of collision energies. This finding highlights the substantial impact of the C–N stretching and H–C–N and/or H–N–C bending modes of the HCN/HNC molecule, as well as the large amplitude motion of the hydrogen atom around the CN molecule in the deep potential well, which were held constant in the 1D model. These factors play a crucial role in the radiative probability and molecule formation. Furthermore, assuming that the QCT method performs similarly in both 1D and full dimension (as it can reproduce the QM cross section baseline), the full-dimensional QCT calculations provide a lower estimate for the exact quantum mechanical cross section due to the absence of resonances.

It has to be stressed that our implementation of the QCT calculations cannot distinguish the formation of HCN and HNC isomers by radiative association. However, as we will see below, this is unnecessary based on the analysis of emission spectra.

C. Emission spectra and the mechanism of radiative association in H + CN collisions

Besides the cross section, our method also allows us to extract the spectrum of the emission in collisions. By using the Wiener–Khinchin theorem, it can be shown that this spectrum is similar to that obtained from the dipole-dipole auto-correlation function, which is usually used to calculate vibrational spectrum from molecular dynamics simulations.[57–59] However, in our case, we calculate a transient (collision induced) vibrational emission spectrum in contrast to the infrared absorption spectrum of stable molecules. This vibrational information of the transient collision complex may shed light on the mechanism of radiative association and how it depends on the collision energy and the initial ro-vibrational state of reactants.

In Fig. 8 the emission spectrum of representative collisions at three different energies is displayed. By analyzing a large number of individual trajectories, we may draw a conclusion about the mechanism of RA process in HCN/HNC system. At high collision energies, the combination bands of the stretching with the bending modes give the biggest contribution to the radiative probability (see Fig. 8 and Table I) which is a clear sign of the strong anharmonicity caused by the high-energy content of the system. This is not surprising, since the timescale of the fast collisions is comparable to the fastest degree of freedom of the system. In most of the energetic collisions, there is no time for several periods of slow modes, as the large amplitude oscillation of H around the CN molecule or the pure C–N stretching. However, when the collision energy is small enough, then efficient pathways are opened for energy flow through the slow degrees of freedom, and the pure harmonic frequencies will appear in the spectrum. Hence, for instance, below E_c = 500 cm^{-1} the harmonic C–H, N–H and C–N stretching modes are dominating (see Fig. 8). Furthermore, in many cases, instead of the bending modes, a large amplitude motion (LAM) can be observed, when the H atom orbits the CN diatom. This LAM can be considerably efficient for RA since the dipole of the system is changing extensively and swiftly.

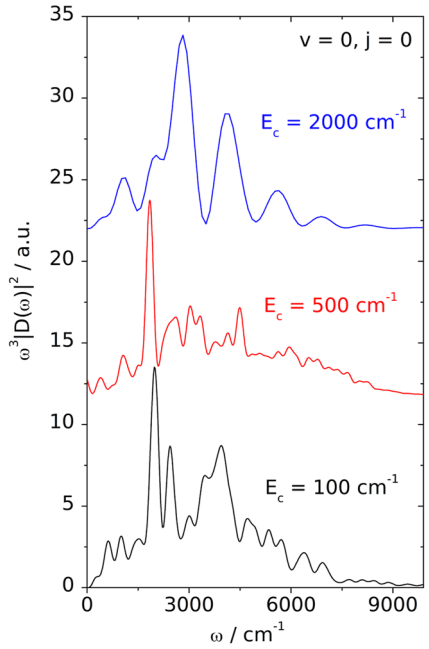

FIG. 8. Normalized spectrum of the radiation for some representative trajectories in H + CN collisions at three different collision energies.

TABLE I. Harmonic vibrational frequencies of the HCN and HNC molecules and their first overtones and combinations.

HCN		HNC	
Mode	ν (cm^{-1})	Mode	ν (cm^{-1})
ν_{CH}	3310	ν_{NH}	3614
ν_{CN}	2081	ν_{CN}	2012
ν_{bend}	704	ν_{bend}	462
$2\nu_{CH}$	6620	$2\nu_{CH}$	7228
$2\nu_{CN}$	4162	$2\nu_{CN}$	4024
$2\nu_{bend}$	1408	$2\nu_{bend}$	924
$\nu_{CH} + \nu_{CN}$	5391	$\nu_{NH} + \nu_{CN}$	5626
$\nu_{CH} + \nu_{bend}$	4014	$\nu_{NH} + \nu_{bend}$	4076
$\nu_{CN} + \nu_{bend}$	2785	$\nu_{CN} + \nu_{bend}$	2474

We can make a significant observation by realizing that the radiative power has a substantial contribution up to ω_{top} = 10 000 cm^{-1} in all collisions (see Fig. 8). This means that the emitted photon carries away a maximum energy of $\hbar\omega_{top}$, and the formed molecule has a maximum binding energy of $E_{bind}^{max} \approx \hbar\omega_{top} - E_c$. Therefore, the formed HCN/HNC system is just below its dissociation limit, with an energy content far exceeding the barrier that separates the HCN and HNC isomers. Based on this, it is not meaningful to distinguish the formation of HCN and HNC molecules in the current QCT calculations. In the interstellar medium, where three-body collisions are negligible, the hot HCN/HNC system formed by radiative association can stabilize in either the HCN or HNC molecule by emitting a second photon.

VI. CONCLUSION

In this work, we have presented an efficient semiclassical method to calculate the detailed dynamics for the formation of arbitrary size molecules by radiative association in absence of electronic transitions. In order to test our method, we also developed a global full-dimensional potential and dipole surface for the H + CN nonreactive collisions. The PES and dipole surface are available as supplementary material. Our method is a combination of the QCT method and the classical Larmor formula, which provides the radiative power in collisions. Owing to the QCT method, we may calculate ro-vibrationally initial quantum state resolved cross sections of RA. We also analyzed the numerical issues regarding the RA calculation using the QCT method and provided solutions for them. Based on our calculation, we have shown that the full-dimensional treatment of the RA process is important, in contrast to previous works where the collision of polyatomic molecules is described solely in 1D. In full dimension, the RA cross section is almost 100 times larger in a wide range of collision energies than that of the reduced dimensional (1D collinear) model. Furthermore, our method also allows us to obtain the emission spectrum of RA process. Analysis of these transient emission spectra can provide the details of the RA mechanism of the molecule in question.

SUPPLEMENTARY MATERIAL

The supplementary material includes the Fortran90 subroutines of the global potential energy and dipole surfaces used in this work. Furthermore, additional figures are also included that support the findings of this works.

ACKNOWLEDGMENTS

This article is based upon work from COST Action Grant No. CA18212—Molecular Dynamics in the GAS phase (MD-GAS), supported by COST (European Cooperation in Science and Technology). The research was funded by the Belgian Science Policy Office (BELSPO), FED-tWIN REVOCS. Furthermore, the support from the Kempe Foundation is gratefully acknowledged. M.G. acknowledges support from the Knut and Alice Wallenberg Foundation. Computational resources provided by the Swedish National Infrastructure for Computing (SNIC) at HPC2N are acknowledged.

AUTHOR DECLARATIONS

Conflict of Interest

The authors have no conflicts to disclose.

Author Contributions

Péter Szabó: Conceptualization (equal); Data curation (equal); Formal analysis (equal); Investigation (equal); Software (equal); Writing – original draft (equal). **Magnus Gustafsson**: Conceptualization (equal); Formal analysis (equal); Funding acquisition (equal);

Resources (equal); Validation (equal); Writing – review & editing (equal).

DATA AVAILABILITY

The data that support the findings of this study are available within the article and its supplementary material.

APPENDIX A: THE UPPER LIMIT OF THE FREQUENCY INTEGRAL AND THE MINIMUM ENERGY RO-VIBRATIONAL STATE OF MOLECULES FORMED BY RADIATIVE ASSOCIATION

The upper limit of the frequency integral, $\omega_{\max}$ in Eqs. (7) and (9)–(11) requires the determining the maximum binding energy (or the minimum energy content) of molecules formed after the emission of a photon by considering the conservation of the total angular momentum (see Fig. 1)

$$\hbar\omega_{\max} = E_c + \max\left[E_{\text{bind}}(\mathbf{J})\right], \tag{A1}$$

where E_c is the collision energy and $E_{\text{bind}}(\mathbf{J})$ is the binding energy of the formed molecule at a given total angular momentum, $\mathbf{J}$, as displayed in Fig. 1.

When the potential energy is deep enough, like in the case of the HCN/HNC molecule, then the value of $\omega_{\max}$ can be chosen smaller than that demanded by the possible maximum binding energy of the molecule with a given angular momentum. Such simplification is possible since for a general molecule the C–H, O–H and N–H stretching are the largest frequency harmonic modes (see e.g., Table I). Furthermore, the overtones and the combination bands of these largest and other lower frequency harmonic modes can give a considerable radiative contribution up to $\omega_{\text{top}} \approx 10\,000$–$15\,000\ \text{cm}^{-1}$ for a general molecule. Therefore, we may approximate the upper limit of the frequency integral in Eqs. (7) and (9)–(11) as $\omega_{\max} = \omega_{\text{top}}$. However, when the potential well of the molecule is shallow (less than $15\,000\ \text{cm}^{-1}$ deep), we have to optimize $E_{\text{bind}}(\mathbf{J})$ at constant $\mathbf{J}$ values. In the remainder of this section, we give a practical solution how to estimate the maximum of $E_{\text{bind}}(\mathbf{J})$ which changes from collision to collision, owing to the varying total angular momentum in different trajectories.

First, we assume that the total internal energy of the molecule – measured from the bottom of the potential well – is separable: $E_{\text{mol}} = E_{\text{vib}} + E_{\text{rot}}$, where

$$E_{\text{vib}} = \sum_{i=1}^{3N-6}\left(\frac{1}{2} + n_i\right)\hbar\nu_i \tag{A2}$$

is assumed to be the sum of quantum mechanical harmonic mode energies, where n_i is the vibrational quantum number and ν_i is the frequency of the ith mode. The rotational energy can be approximated as the energy of a classical 3D rigid-rotor (RR)

$$E_{\text{rot}} = \frac{1}{2}\mathbf{J}^{\mathrm{T}}\mathbf{I}^{-1}\mathbf{J}, \tag{A3}$$

where $\mathbf{J}$ is the total angular momentum of the formed molecules in the A + B → AB + $\hbar\omega$ collisions, and $\mathbf{I}$ is the tensor of inertia of the AB molecule. By considering that the emitted photon takes away $1\hbar$ angular momentum, owing to its bosonic nature, the total angular momentum of the formed molecules in the A + B → AB + $\hbar\omega$ collisions is

$$\mathbf{J} = \mathbf{L}_{\text{orb}} + \mathbf{J}_{\text{A}} + \mathbf{J}_{\text{B}} - \hbar\mathbf{E} \tag{A4}$$

where $\mathbf{L}_{\text{orb}}$ is the orbital angular momentum, $\mathbf{J}_{\text{A}}$ and $\mathbf{J}_{\text{B}}$ are the rotational angular momenta of the fragment A and B. Furthermore, $\mathbf{E}$ is a unit vector that determines the direction of the angular momentum of the emitted photon. The rotational quantum numbers, j_{A} and j_{B} determine the magnitude of $|\mathbf{J}_{\text{A}}| = \hbar\sqrt{j_{\text{A}}(j_{\text{A}}+1)}$ and $|\mathbf{J}_{\text{B}}| = \hbar\sqrt{j_{\text{B}}(j_{\text{B}}+1)}$, while their orientation is sampled randomly, which means it is different for each trajectory. The impact parameter, b and collision energy determine the magnitude of the orbital angular momentum

$$|\mathbf{L}_{\text{orb}}| = b\sqrt{2\mu E_c}, \tag{A5}$$

while its well-defined orientation depends on the simulation setup. Moreover, the orientation of the angular momentum, $\mathbf{E}$, taken by the photon is also supposed to be sampled randomly. Based on these considerations, the possible energy content of the molecules formed in the RA process depends on the initial conditions of the reactants, owing to the varying orientation of the angular momenta. In order to find $\omega_{\max}$, we have to minimize $E_{\text{mol}} = E_{\text{vib}} + E_{\text{rot}}$ at certain $\mathbf{J}$ values. By using the harmonic oscillator (HO) approximation in Eq. (A2), we have to minimize E_{mol} along the normal mode coordinates. Hence, by optimizing the value of vibrational quantum numbers, $(n_1, n_2, \ldots, n_{3N-6})$ as well as the rotational energy along the normal coordinates at each fixed set of vibrational quantum numbers, we obtain the maximum frequency as

$$\hbar\omega_{\max} = E_c + E_0^{\text{eq}} - \min\left[E_{\text{vib}} + E_{\text{rot}}\right], \tag{A6}$$

where E_0^{eq} is the depth, to the global minimum, of the potential well. Furthermore, the amplitude of the normal modes is determined by the vibrational quantum numbers. This procedure can provide the exact $\omega_{\max}$ within the HO-RR approximation. This minimization is supposed to be done for every trajectory, which can be computationally expensive for bigger molecules.

In order to provide a simpler estimation of $\omega_{\max}$, we assume that the minimum of E_{mol} is at the zero-point vibration level of the lowest energy isomer of the formed molecule (corresponding to the absolute minimum of the PES) regardless of the rotational energy. Furthermore, to avoid the minimization along the normal coordinates, we may assume that the minimum of the rotational energy (at a given $\mathbf{J}$) is at the equilibrium structure of the molecule. Hence, the maximum frequency of the emitted photon in a polyatomic RA process can be estimated as

$$\hbar\omega_{\max} \approx E_c + E_0^{\text{eq}} - \frac{1}{2}\sum_{i=1}^{3N-6}\hbar\nu_i - \frac{1}{2}\mathbf{J}^{\mathrm{T}}\mathbf{I}_{\text{eq}}^{-1}\mathbf{J}, \tag{A7}$$

where $\mathbf{I}_{\text{eq}}$ is the tensor of inertia at the equilibrium geometry.

APPENDIX B: CORRECTION OF THE DIPOLE FOR NON-INTERACTING REACTANTS

When one wants to use Eq. (11) to obtain the correct radiative power that results in molecule formation, then the radiation of the non-interactive reactants can be eliminated by using the induced

dipole outside the interaction zone and the total dipole inside the zone. Thus, the corresponding dipole is

$$\mathbf{D}(\mathbf{q},t) = \begin{cases} \widetilde{\mathbf{D}}(\mathbf{q},t) - \widetilde{\mathbf{D}}_0(\mathbf{q},0) & \text{if} \quad \mathbf{q} \notin [\text{int. zone}] \\ \widetilde{\mathbf{D}}(\mathbf{q},t) & \text{if} \quad \mathbf{q} \in [\text{int. zone}], \end{cases} \tag{A8}$$

where $\widetilde{\mathbf{D}}_0(\mathbf{q},0)$ is the dipole of the non-interacting fragments at a given $\mathbf{q}$ molecular arrangement at time $t = 0$. This is illustrated by non-zero value of D_z for H far away in Fig. 4(a). In the transition from inside to outside the interaction zone a switching function is applied as described for the alternative method in Sec. III B 1.

APPENDIX C: QUANTUM MECHANICAL PERTURBATION THEORY

The quantum mechanical perturbation theory treatment of the radiative stabilization yields a Golden rule-like formula for the cross section[2,98]

$$\sigma(E_c) = \frac{64\pi^5 f_{\text{stat}}}{3k_{\text{ini}}^2 4\pi\epsilon_0} \sum_{J,j',v'} \frac{S_{J,j'}}{\lambda^3_{J,j',v',E_c}} \left|M_{J,j',v',E_c}\right|^2, \tag{A9}$$

where the sum runs over the initial angular momentum (J) and final rotational (j') and vibrational (v') quantum numbers. $k_{\text{ini}} = \sqrt{(2\,\mu E_c)}/\hbar$ is the wavenumber, where μ is the reduced mass of the colliding fragments, $S_{J,j'}$ is the Hönl–London factor, λ_{J,j',v',E_c} is the wavelength of the emitted photon. The transition dipole matrix elements are defined as

$$M_{J,j',v',E_c} = \left\langle \varphi^{\text{fin}}_{j',v'}(r) \middle| \hat{D}(r) \middle| \chi^{\text{ini}}_{J,E_c}(r) \right\rangle, \tag{A10}$$

where $\hat{D}(r)$ is the operator of the dipole moment function, $\chi^{\text{ini}}_{J,E_c}(r)$ is the radial part of the energy normalized scattering wavefunction of the initial state and $\varphi^{\text{fin}}_{j',v'}(r)$ is the radial part of the final ro-vibrational wavefunction, normalized to unity.

REFERENCES

[1] J. F. Babb and K. P. Kirby, in *The Molecular Astrophysics of Stars and Galaxies*, edited by T. W. Hartquist and D. A. Williams (Clarendon Press, Oxford, 1998), p. 11.
[2] G. Nyman, M. Gustafsson, and S. V. Antipov, Int. Rev. Phys. Chem. **34**, 385 (2015).
[3] D. Gerlich and S. Horning, Chem. Rev. **92**, 1509 (1992).
[4] M. Gustafsson, M. Monge-Palacios, and G. Nyman, J. Chem. Phys. **140**, 184301 (2014).
[5] J. Franz, M. Gustafsson, and G. Nyman, Mon. Not. R. Astron. Soc. **414**, 3547 (2011).
[6] P. D. Singh and C. M. Andreazza, Astrophys. J. **537**, 261 (2000).
[7] G. Barinovs and M. C. van Hemert, Astrophys. J. **636**, 923 (2006).
[8] R. C. Forrey, J. F. Babb, P. C. Stancil, and B. M. McLaughlin, Mon. Not. R. Astron. Soc. **479**, 4727 (2018).
[9] J. F. Babb and B. M. McLaughlin, Mon. Not. R. Astron. Soc. **468**, 2052 (2017).
[10] J. F. Babb, R. T. Smyth, and B. M. McLaughlin, Astrophys. J. **884**, 155 (2019).
[11] J. F. Babb, R. T. Smyth, and B. M. McLaughlin, Astrophys. J. **876**, 38 (2019).
[12] P. Szabó and M. Gustafsson, Mon. Not. R. Astron. Soc. **483**, 3574 (2018).
[13] M. Zámečníková, P. Soldán, M. Gustafsson, and G. Nyman, Mon. Not. R. Astron. Soc. **489**, 2954 (2019).
[14] M. Zámečníková, M. Gustafsson, G. Nyman, and P. Soldán, Mon. Not. R. Astron. Soc. **492**, 3794 (2020).
[15] R. K. Kathir, G. Nyman, and M. Gustafsson, Mon. Not. R. Astron. Soc. **470**, 3068 (2017).
[16] C. M. Andreazza, A. A. de Almeida, R. M. Vichietti, and D. T. Ceccatto, Mon. Not. R. Astron. Soc. **427**, 833 (2012).
[17] C. M. Andreazza, A. A. de Almeida, and R. M. Vichietti, Mon. Not. R. Astron. Soc. **477**, 548 (2018).
[18] C. M. Andreazza, A. A. de Almeida, and A. C. Borin, Mon. Not. R. Astron. Soc. **457**, 3096 (2016).
[19] C. M. Andreazza and A. A. de Almeida, Mon. Not. R. Astron. Soc. **437**, 2932 (2014).
[20] J. Öström, D. S. Bezrukov, G. Nyman, and M. Gustafsson, J. Chem. Phys. **144**, 044302 (2016).
[21] S. V. Antipov, T. Sjölander, G. Nyman, and M. Gustafsson, J. Chem. Phys. **131**, 074302 (2009).
[22] S. V. Antipov, M. Gustafsson, and G. Nyman, J. Chem. Phys. **135**, 184302 (2011).
[23] O. J. Bennett, A. S. Dickinson, T. Leininger, and F. X. Gadéa, Mon. Not. R. Astron. Soc. **341**, 361 (2003); Erratum **384**, 1743 (2008).
[24] A. S. Dickinson, J. Phys. B: At., Mol. Opt. Phys. **38**, 4329 (2005); Corrigendum **41**, 049801 (2008).
[25] M. Gustafsson and G. Nyman, Mon. Not. R. Astron. Soc. **448**, 2562 (2015).
[26] M. Gustafsson, S. V. Antipov, J. Franz, and G. Nyman, J. Chem. Phys. **137**, 104301 (2012).
[27] T. Bai, Z. Qin, and L. Liu, Mon. Not. R. Astron. Soc. **500**, 2496 (2020).
[28] Z. Qin, T. Bai, and L. Liu, Mon. Not. R. Astron. Soc. **507**, 2930 (2021).
[29] P. Szabó, S. Góger, and M. Gustafsson, Front. Astron. Space Sci. **8**, 704953 (2021).
[30] M. Gustafsson, J. Chem. Phys. **153**, 114305 (2020).
[31] M. Gustafsson and R. C. Forrey, J. Chem. Phys. **150**, 224301 (2019).
[32] D. Jones (nee Burdakova), M. Gustafsson, and G. Nyman, Mon. Not. R. Astron. Soc. **517**, 4892 (2022).
[33] Z. Hou, Z. Qin, and L. Liu, Astron. Astrophys. **672**, A25 (2023).
[34] Z. Qin, P. Hu, J. Li, and L. Liu, Mon. Not. R. Astron. Soc. **523**, 2684 (2023).
[35] M. Šimsová née Zámečníková, M. Gustafsson, and P. Soldán, Phys. Chem. Chem. Phys. **24**, 25250 (2022).
[36] M. Simsová-Zámecníková, P. Soldán, and M. Gustafsson, Astron. Astrophys. **664**, A5 (2022).
[37] F. Mrugała, V. Špirko, and W. P. Kraemer, J. Chem. Phys. **118**, 10547 (2003).
[38] F. Mrugała and W. P. Kraemer, J. Chem. Phys. **122**, 224321 (2005).
[39] F. Mrugała and W. P. Kraemer, J. Chem. Phys. **138**, 104315 (2013).
[40] T. Stoecklin, F. Lique, and M. Hochlaf, Phys. Chem. Chem. Phys. **15**, 13818 (2013).
[41] M. Ayouz, R. Lopes, M. Raoult, O. Dulieu, and V. Kokoouline, Phys. Rev. A **83**, 052712 (2011).
[42] D. Burdakova, G. Nyman, and T. Stoecklin, Mon. Not. R. Astron. Soc. **485**, 5874 (2019).
[43] D. Jones (nee Burdakova), G. Nyman, and T. Stoecklin, Mon. Not. R. Astron. Soc. **503**, 3089 (2021).
[44] T. Stoecklin, P. Halvick, H.-G. Yu, G. Nyman, and Y. Ellinger, Mon. Not. R. Astron. Soc. **475**, 2545 (2017).
[45] D. Talbi and M.-C. Bacchus-Montabonel, Chem. Phys. Lett. **485**, 56 (2010).
[46] A. Tajti, G. Lendvay, and P. G. Szalay, J. Phys. Chem. Lett. **8**, 3356 (2017).
[47] E. Herbst and R. C. Dunbar, Mon. Not. R. Astron. Soc. **253**, 341 (1991).
[48] E. Herbst, Astron. Astrophys. **153**, 151 (1985), available at https://ui.adsabs.harvard.edu/abs/1985A & A...153..151H.
[49] E. Herbst, Astrophys. J. **292**, 484 (1985).
[50] E. Herbst and K. Yamashita, J. Chem. Soc., Faraday Trans. **89**, 2175 (1993).
[51] J. Cernicharo, C. Cabezas, J. R. Pardo, M. Agúndez, O. Roncero, B. Tercero, N. Marcelino, M. Guélin, Y. Endo, and P. de Vicente, Astron. Astrophys. **672**, L13 (2023).
[52] P. Szabó and G. Lendvay, J. Phys. Chem. A **119**, 7180–7189 (2015).
[53] P. Szabó and G. Lendvay, J. Phys. Chem. A **119**, 12485 (2015).
[54] S. Góger, P. Szabó, G. Czakó, and G. Lendvay, Energy Fuels **32**, 10100 (2018).

[55]D. Gao, X. Xin, D. Wang, P. Szabó, and G. Lendvay, Phys. Chem. Chem. Phys. **24**, 10548 (2022).
[56]B. Csorba, P. Szabó, S. Góger, and G. Lendvay, J. Phys. Chem. A **125**, 8386 (2021).
[57]W. Fakhardji, P. Szabó, M. S. A. El-Kader, A. Haskopoulos, G. Maroulis, and M. Gustafsson, J. Chem. Phys. **151**, 144303 (2019).
[58]W. Fakhardji, P. Szabó, M. S. A. El-Kader, and M. Gustafsson, J. Chem. Phys. **152**, 234302 (2020).
[59]W. Fakhardji, P. Szabó, and M. Gustafsson, J. Quant. Spectrosc. Radiat. Transfer **276**, 107926 (2021).
[60]D. N. Chistikov, A. A. Finenko, S. E. Lokshtanov, S. V. Petrov, and A. A. Vigasin, J. Chem. Phys. **151**, 194106 (2019).
[61]D. N. Chistikov, A. A. Finenko, Y. N. Kalugina, S. E. Lokshtanov, S. V. Petrov, and A. A. Vigasin, J. Chem. Phys. **155**, 064301 (2021).
[62]Y. Bedjanian, P. Szabó, and G. Lendvay, J. Phys. Chem. A **127**, 6916 (2023).
[63]M. Gustafsson, J. Chem. Phys. **138**, 074308 (2013).
[64]P. Szabó and M. Gustafsson, J. Chem. Phys. **147**, 094308 (2017).
[65]R. Glaser, B. Hodgen, D. Farrelly, and E. McKee, Astrobiology **7**, 455 (2007).
[66]W. M. Irvine, Space Sci. Rev. **90**, 203 (1999).
[67]J. S. Greaves and S. E. Church, Mon. Not. R. Astron. Soc. **283**, 1179 (1996).
[68]R. C. Young Owl, M. M. Meixner, M. Wolfire, A. G. G. M. Tielens, and J. Tauber, Astrophys. J. **540**, 886 (2000).
[69]D. Johnstone, A. M. S. Boonman, and E. F. van Dishoeck, Astron. Astrophys. **412**, 157 (2003).
[70]A. Fuente, S. Garcia-Burillo, M. Gerin, D. Teyssier, A. Usero, J. R. Rizzo, and P. de Vicente, Astrophys. J. **619**, L155 (2005).
[71]R. Bachiller, T. Forveille, P. J. Huggins, and P. Cox, Astron. Astrophys. **324**, 1123 (1997), available at https://adsabs.harvard.edu/full/1997A%26A...324.1123B.
[72]W.-F. Thi, G.-J. van Zadelhoff, and E. F. van Dishoeck, Astron. Astrophys. **425**, 955 (2004).
[73]R. D. Brown, F. R. Burden, and A. Cuno, Astrophys. J. **347**, 855 (1989).
[74]G. I. Boger and A. Sternberg, Astrophys. J. **632**, 302 (2005).
[75]F. Borget, S. Müller, D. Grote, P. Theulé, V. Vinogradoff, T. Chiavassa, and W. Sander, Astron. Astrophys. **598**, A22 (2017).
[76]Z. Homayoon, S. A. Vazquez, R. Rodríguez-Fernandez, and E. Martínez-Nunez, J. Phys. Chem. A **115**, 979 (2011).
[77]A. Haca, A. D. Bosman, and E. F. van Dishoeck, Astron. Astrophys. **635**, A4 (2020).
[78]D. R. Bates, Mon. Not. R. Astron. Soc. **111**, 303 (1951).
[79]B. Zygelman and A. Dalgarno, Phys. Rev. A **38**, 1877 (1988).
[80]L. D. Landau and E. M. Lifsitz, *The Classical Theory of Fields*, 4th ed., *Course of Theoretical Physics Vol. 2* (Butterworth-Heinemann, 1980).
[81]R. N. Porter, L. M. Raff, and W. H. Miller, J. Chem. Phys. **63**, 2214 (1975).
[82]T. Nagy and G. Lendvay, J. Phys. Chem. Lett. **8**, 4621 (2017).
[83]G. Czakó, J. Phys. Chem. A **116**, 7467 (2012).
[84]J. Kopp, Int. J. Mod. Phys. C **19**, 523 (2008).
[85]A. Savitzky and M. J. E. Golay, Anal. Chem. **36**, 1627 (1964).
[86]H.-J. Werner *et al.*, MOLPRO, version 2015.1, a package of *ab initio* programs, 2015.
[87]W. Schadow, B-spline library version 2.2, http://www.wolfgangschadow.com/software, 2000.
[88]M. Ayouz, O. Dulieu, R. Guérout, J. Robert, and V. Kokoouline, J. Chem. Phys. **132**, 194309 (2010).
[89]J. Tennyson, M. A. Kostin, P. Barletta, G. J. Harris, O. L. Polyansky, J. Ramanlal, and N. F. Zobov, Comput. Phys. Commun. **163**, 85 (2004).
[90]T. van Mourik, G. J. Harris, O. L. Polyansky, J. Tennyson, A. G. Császár, and P. J. Knowles, J. Chem. Phys. **115**, 3706 (2001).
[91]A. Chenel, O. Roncero, A. Aguado, M. Agúndez, and J. Cernicharo, J. Chem. Phys. **144**, 144306 (2016).
[92]A. J. C. Varandas and S. P. J. Rodrigues, J. Phys. Chem. A **110**, 485 (2006).
[93]B. Mehnen, I. Suarez Martin, E. Roueff, M. Hochlaf, and G. Nyman, Mon. Not. R. Astron. Soc. **517**, 3126 (2022).
[94]V. Y. Makhnev, A. A. Kyuberis, N. F. Zobov, L. Lodi, J. Tennyson, and O. L. Polyansky, J. Phys. Chem. A **122**, 1326 (2018).
[95]G. C. Mellau, J. Chem. Phys. **134**, 234303 (2011).
[96]A. Vikár, T. Nagy, and G. Lendvay, J. Phys. Chem. A **120**, 5083 (2016).
[97]T. Nagy, A. Vikár, and G. Lendvay, Phys. Chem. Chem. Phys. **20**, 13224 (2018).
[98]J. F. Babb and A. Dalgarno, Phys. Rev. A **51**, 3021 (1995).